Biosensors and Bioelectronics 126 (2019) 88–95

Contents lists available at ScienceDirect

Biosensors and Bioelectronics

journal homepage: www.elsevier.com/locate/bios

Label free thrombin detection in presence of high concentration of albumin using an aptamer-functionalized nanoporous membrane

Agnivo Gosai[a], Brendan Shin Hau Yeah[a], Marit Nilsen-Hamilton[b,c], Pranav Shrotriya[a,*]

[a] Department of Mechanical Engineering,Iowa State University, 2019 Black Engineering Building, Ames, IA 50011, United States
[b] Department of Biochemistry, Biophysics and Molecular Biology, Iowa State University, Ames, IA 50011, United States
[c] Aptalogic Inc, United States

ARTICLE INFO

Keywords:
Thrombin
Aptamer
EIS
Nanoporous alumina membrane
Serum albumin

ABSTRACT

Nanoporous alumina membranes have become a ubiquitous biosensing platform for a variety of applications and aptamers are being increasingly utilized as recognition elements in protein sensing devices. Combining the advantages of the two, we report label-free sensitive detection of human α-thrombin by an aptamer-functionalized nanoporous alumina membrane using a four-electrode electrochemical cell. The sensor response to α-thrombin was determined in the presence of a high concentration (500 μM) of human serum albumin (HSA) as an interfering protein in the background. The sensor sensitivity was also characterized against γ-thrombin, which is a modified α-thrombin lacking the aptamer binding epitope. The detection limit, within an appreciable signal/noise ratio, was 10 pM of α-thrombin in presence of 500 μM HSA. The proposed scheme involves the use of minimum reagents/sample preparation steps, has appreciable response in presence of high concentrations of interfering molecules and is readily amenable to miniaturization by association with existing-chip based electrical systems for application in point-of-care diagnostic devices.

1. Introduction

Nanoporous anodized alumina or aluminum oxide (NAAO) membranes are increasingly assuming an important role in chemical/biological sensing due to several desirable properties like non-conductivity, structured nanopores, high pore density as well as surface to volume ratio, and ease of functionalization (Santos et al., 2013). NAAO membranes thus have exciting potential in biosensing devices through miniaturization and integration into lab-on-chip and point-of-care diagnostic systems. NAAO membranes have found application as biosensor platforms in several niche biosensing areas including nucleic acid sensing (Ye et al., 2014; Rai et al., 2012), detection of bacteria (Wang et al., 2009; Tan et al., 2011), virus particles (Chaturvedi et al., 2016), antibody (de la Escosura-Muñiz and Merkoçi, 2010) and protein sensing (de la Escosura-Muñiz et al., 2013).

The hallmark of a good biosensor is a reliable receptor or recognition element apart from the robust sensing platform. In this regard, nucleic acid aptamers are prime candidates for recognition elements towards target analyte (e.g. proteins) in many biosensing devices (Du and Dong, 2017). Aptamers are short oligonucleotides that are being increasingly investigated for biosensing due to their high affinities, specificities, small sizes, robustness for handling/storage in terms of adaptability to a wide range of temperatures. They can potentially replace antibodies for analytical and therapeutic applications (Deng et al., 2014; Ilgu and Nilsen-Hamilton, 2016). Aptamer-based sensors have been previously used in both labeled or label-free devices (Daniels and Pourmand, 2007).

Label-free biosensing techniques involve detection of target-probe binding, which can provide information on binding kinetics, association/dissociation rates and constants and determine binding/unbinding events. In particular, label-free electrochemical impedance spectroscopy (EIS) based characterization techniques (Daniels and Pourmand, 2007) offer great flexibility in the incorporation of NAAO membranes into existing detection schemes and could facilitate the realization of parallel/multiplexed assays. The issue of selective detection is of paramount importance for a bio-sensor devised for real-world application where the target concentration can be much lower than the concentrations of non-target biomolecules. This demands thorough consideration in improving the efficacy of such sensors.

In this study, we have determined the sensitive label-free detection of human α-thrombin with an aptamer modified NAAO in a custom-made four-electrode electrochemical cell (Fig. 1C) using the EIS technique. Previously Escosura-Muniz et al.,(de la Escosura-Muñiz et al., 2013) achieved a low concentration sensing of α-thrombin in whole

* Corresponding author.
E-mail address: shrotriy@iastate.edu (P. Shrotriya).

https://doi.org/10.1016/j.bios.2018.10.010
Received 23 July 2018; Received in revised form 21 September 2018; Accepted 3 October 2018
Available online 18 October 2018
0956-5663/

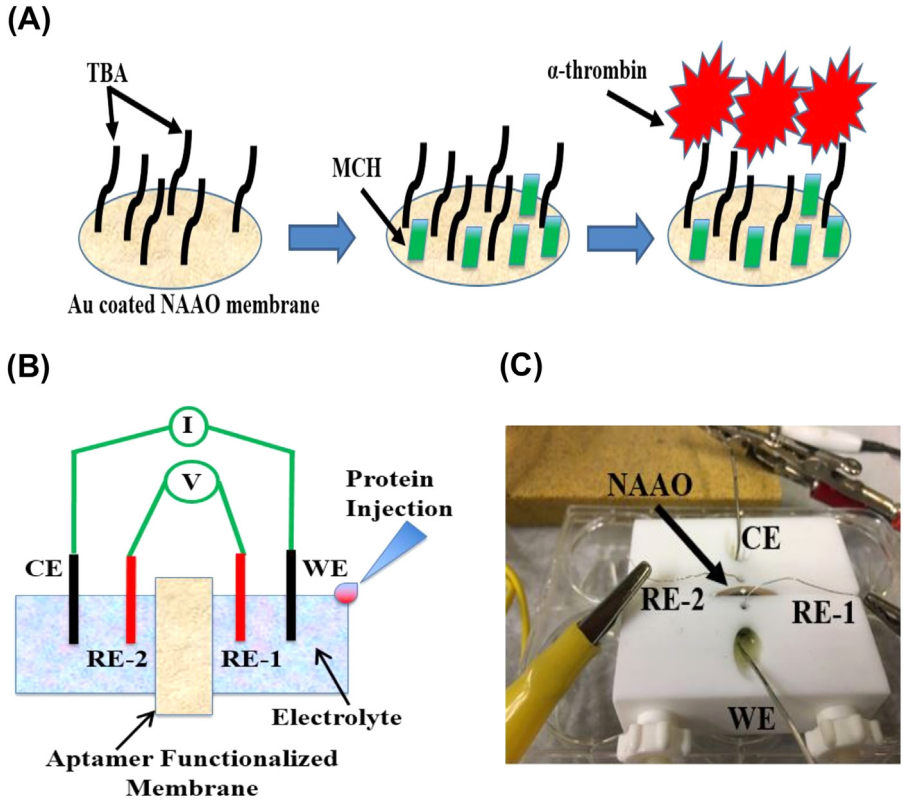

Fig. 1. (A) Schematic showing membrane immobilization steps (B) The four-electrode scheme is shown (C) the Teflon cell as used in the electrochemical experiments with the NAAO membrane and the four-electrode set-up.

blood using gold nanoparticle-based aptamer sandwich systems in NAAO membrane pores. In their work, the NAAO membrane is the working electrode in the electrochemical system, in which the biomolecular complex attached to the surface of the NAAO membrane may be influenced due to the direct effect of the electric field created by the electrode. In fact, the actuation/modulation of nucleic acid and their ligands due to electric field has been previously reported to be capable of affecting the sensor response. To avoid this effect, we have devised an indirect method to measure the impedance changes on the membrane by using a four-electrode set-up. Recently, Zhao et al. (2017) reported the label-free detection of α-thrombin by an aptamer-modified NAAO membrane using a two-electrode method, but they did not test the detection efficacy in the presence of interfering proteins. Also, in the four-electrode method the voltage-measuring electrodes are not under the effect of the current-carrying outer electrodes and thus have better measurement accuracy than with a two-electrode system.

Under physiological conditions in human blood, the α-thrombin concentration can range from a few nanomolar (nM) (unperturbed blood) to a few hundred nM (when the clotting cascade is activated) (Aronson et al., 1977). The sensitivity of the proposed sensor has been rigorously investigated for physiologically relevant α-thrombin concentrations in presence of a high background of 500 micromolar (μM) human serum albumin (HSA) (the physiological concentration of HSA ~ 500–700 μM) (Wang et al., 2012). HSA is the most abundant protein in human serum, makes up close to 60% of blood plasma proteins and is a major contributor to non-specific interactions for biosensors. We also utilized γ-thrombin as a negative control, which is analogous in structure to α-thrombin but lacks the residues for selective binding to the aptamer.

By testing our aptamer-based sensor in presence of high concentration HSA we can effectively establish the specificity and selectivity of the proposed sensing scheme. The novelty of our design scheme lies in label-free detection using minimal sample preparation steps and the ease of miniaturization for integration with point-of-care diagnostic devices focusing on improved specificity and selectivity.

2. Experimental methods

2.1. Materials

The NAAO (Sigma Aldrich, Whatman), having nominal pore diameters of 20 nm and membrane thickness of 50 μm, were used for the experiments. This membrane was chosen based on earlier reports and with respect to the sizes of the biomolecules involved (Kant et al., 2014a, 2014b; Tagliazucchi et al., 2011). Thiolated thrombin-binding aptamer (TBA) was obtained from Integrated DNA Technologies (IDT) with the sequence 5′-/5ThioMC6-D/GCCTTAACTGTAGTACTGGTGAA ATTGCTGCCATT**GGTT GGTGTGGTTGG**-3′. The bold letters denote the aptamer sequence that binds selectively to human α-thrombin (Bock et al., 1992; Schultze et al., 1994). Human α-thrombin, γ-thrombin, serum albumin (HSA), lysozyme, and 6-mercapto-1-hexanol (MCH) were procured from Thermo-Fisher Scientific. The electrolyte used for sensing experiments was 1 mM $Fe(CN)_6^{4-}$/$Fe(CN)_6^{3-}$redox couple in PBS (137 mM NaCl, 2.7 mM KCl, 10 mM Na_2HPO_4, 2 mM KH_2PO_4, 5 mM $MgCl_2$, pH 7.4 at room temperature). All the chemicals used for electrolyte were purchased from Sigma-Aldrich. All solutions were prepared with double distilled water (ddH_2O) produced by a Corning Mega-Pure system.

2.2. Preparing membranes for experimentation

The NAAO membranes were cleaned/sonicated with isopropanol, ethanol and ddH_2O. Afterwards, one side of the membranes was sputter-coated with 60 nm of gold, followed by washing with isopropanol, ethanol and ddH_2O. Gold coated NAAO membranes have been utilized previously in several studies discussing biosensing

applications (Li et al., 2018a; Li et al., 2018b; Macias et al., 2013; Toccafondi et al., 2016; Kumeria et al., 2014) and can be readily functionalized by thiolated receptors through chemical self-assembly (Ma et al., 2017). The TBA received from IDT was brought to 1 μM in PS buffer (PBS without $MgCl_2$) and stored refrigerated. Before an experiment an aliquot was heated to 90 °C, $MgCl_2$ was added and the solution was allowed to slowly cool down to room temperature before being put on the gold coated NAAO membrane, which was then left at 4 °C for 12 h to immobilize the TBA. The NAAO membrane was washed with PBS and further incubated for 1 h at room temperature with 3 mM MCH in ddH_2O to passivate the surface followed by washing with PBS. These steps are represented graphically in Fig. 1A.

2.3. Electrochemical sensing

For all electrochemical experiments a custom-made Teflon cell (Fig. 1C) was used. The four-electrode method was utilized to measure the impedance changes for the NAAO membrane (represented in Fig. 1B). Platinum wires were used for the working (WE) and counter electrodes (CE) whereas Ag/AgCl wires (Invivometric) were used as the two reference electrodes (RE). EIS was carried out with an AC perturbation signal of 5 mV over a DC potential equal to the open circuit potential of the system, within the frequency range of 10 kHz-0.1 Hz. Equal volumes of protein solution (α-thrombin as analyte and other proteins for negative controls) prepared in PBS were injected onto the port of the Teflon cell containing the TBA functionalized side of the membrane (Fig. 1B). The concentration of each injection was determined to achieve the desired target concentration inside the electrochemical cell to obtain a calibration curve for the titration experiment. EIS was carried out after 30 min to provide ample time for diffusion of protein based on the reported association constant of α-thrombin and its aptamer (Li et al., 2008). The system was tested separately for selectivity for α-thrombin compared with γ-thrombin and HSA as negative controls. It was also tested for specificity for α-thrombin over γ-thrombin and lysozyme in the presence of 500 μM HSA as the interfering protein.

3. Experimental results and discussion

3.1. Characterization of impedance change

Figs. 2A and 2B show the frequency responses i.e. the Bode plot and the Nyquist plots of the system, respectively, where the responses to different proteins at 10 nM were determined for separate experiments. The data in Fig. 2A contains a significant contribution from the solution resistance, which is influenced by the different charges on the proteins. This solution impedance dominates more at the higher frequencies of the AC perturbation voltage used in EIS. The system impedance Z_{system} does not explicitly capture the effect of aptamer-protein impedance occurring on the membrane surface. To better understand the changes occurring on the membrane it is useful to analyze the Nyquist plots in Fig. 2B in which the solution impedance is subtracted from the real axis of the Nyquist plot. From Fig. 2B it is observed that the shape of the Nyquist plot for α-thrombin (analyte) was appreciably different from the shape with no protein, whereas those for γ-thrombin and HSA (negative controls) were more closely aligned with the latter plot. The

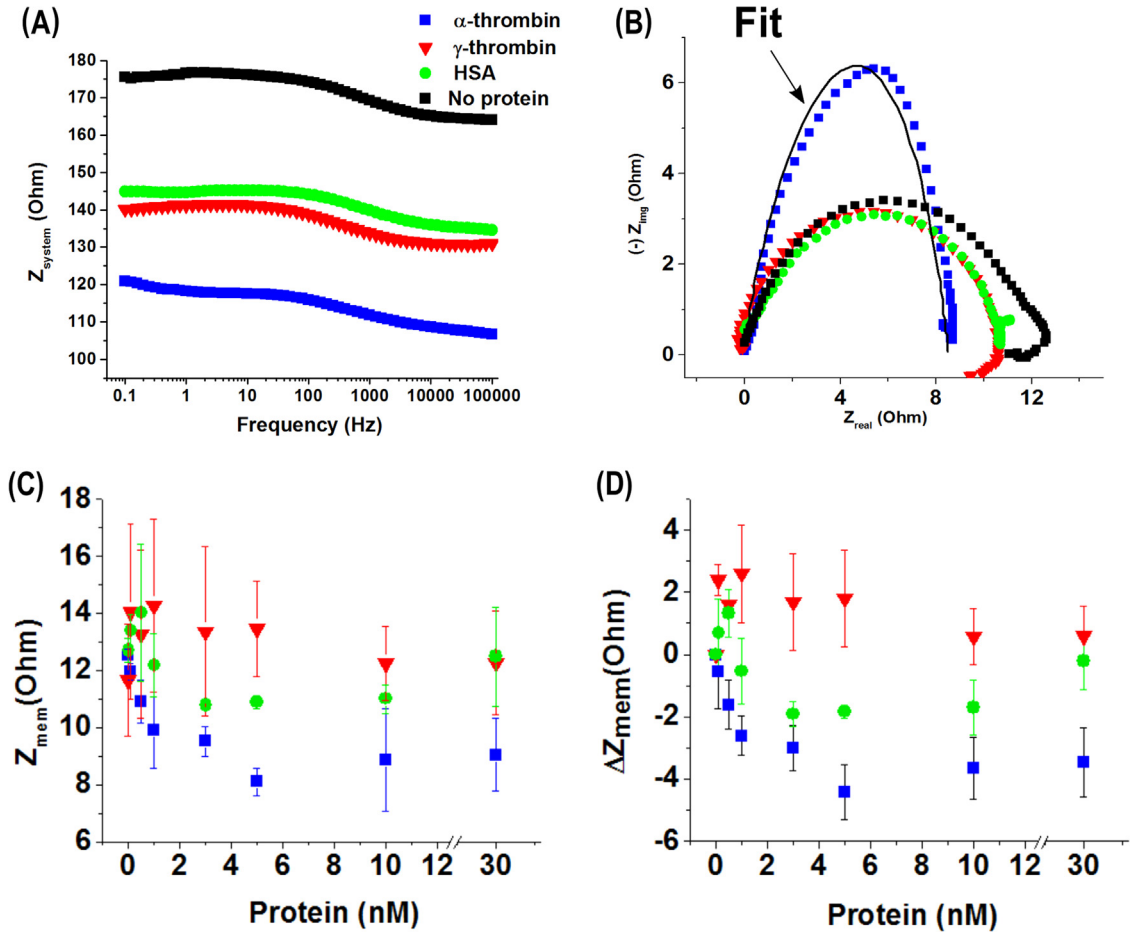

Fig. 2. (A) A representative frequency response (Bode plot) and (B) a representative Nyquist plot, at 10 nM concentration of different proteins. The black curve on the Nyquist plot is the modified Randle's circuit fit for α-thrombin; (C) the membrane impedance Z_{mem} and (D) ΔZ_{mem} is plotted of the aptamer functionalized membrane for different protein concentrations. Each titration experiment was repeated at least 3 times. The error bars correspond to standard deviation of the mean.

EIS data, in the form of Bode plots (Fig. 2A) and Nyquist plots (Fig. 2B), were fit to the modified Randle's circuit (explained in Supplementary information S1) and the relevant membrane parameters, namely pore resistance R_p and membrane capacitance C_{mem} were extracted. Supplementary Figs. S3A and S3B show the R_p and C_{mem} for the α-thrombin, γ-thrombin and HSA titrations. It is observed that, at lower protein concentrations, the data for R_p and particularly that for C_{mem} had less resolution. As the titration progressed, R_p decreased appreciably with the selective and specific binding of α-thrombin to TBA. Due to more charges accumulating on the membrane resulting from the α-thrombin-TBA complex, C_{mem} increased progressively. The response for the negative controls did not scale to the same extent. The membrane impedance Z_{mem} (depicted in Fig. 2C) was calculated for a frequency $f = 100$ Hz (chosen from Fig. 2A as an inflection point of the frequency response curve) and this data, as plotted in Fig. 2C shows better resolution compared to the separate R_p and C_{mem} data.

Z_{mem} was calculated as below:

$$Z_{mem} = \frac{1}{\sqrt{\left(\frac{1}{R_p}\right)^2 + (2\pi f C_{mem})^2}}$$

To further resolve the response, the difference in impedance $(Z_{mem})_{final}$-$(Z_{mem})_{zero\ concentration} = \Delta Z_{mem}$ was calculated for each of the concentrations of protein and plotted against protein concentration (Fig. 2D). This plot improved the distinction of the response at lower α-thrombin concentrations (i.e. 0.1 nM and 0.5 nM) compared with the negative controls.

As a further test, ΔZ_{mem} was monitored over time for certain concentrations of α-thrombin injected into the system for three different cases: (i) system without any membrane (ii) gold coated membrane functionalized with only MCH and (iii) gold coated membrane functionalized with TBA and later passivated with MCH. The results from the experiments with 5 nM of α-thrombin injection into the system suggest that only the TBA functionalized membrane responds appreciably (Supplementary information S2), thus validating the proper functionalization of TBA on the membrane.

3.2. Sensitivity in presence of a high concentration of interfering protein

The system was further tested in presence of a high concentration of HSA (500 μM), the most abundant blood protein, as an interfering protein. In absence of whole blood, this is deemed as a rigorous test for the sensor with a focus to real world applications. With HSA present as an interfering protein, human lysozyme (also positively charged like α-thrombin) was chosen as another negative control. Thus, we have tested for both structural and charge similarities by using γ-thrombin and lysozyme respectively. In Fig. 3A, the membrane impedance Z_{mem} is plotted for the different proteins tested and it may be observed that below 2 nM, the error bars for the responses from α-thrombin and γ-thrombin overlap. From Fig. 3B we observe that the sensor functions well for both the higher and lower concentration zones. In fact, an appreciable response was achieved for 10 pM α-thrombin considering signal/noise ratio as described in the following section. When ΔZ_{mem} is considered as the sensor response it is observed from Fig. 3 B that, below 3 nM concentration, the error bars for the response from γ-thrombin still overlap with the confidence interval for α-thrombin titration. Hence it may be claimed that the sensor is able to detect α-thrombin over 2 nM concentration with 95% confidence in presence of high albumin concentration. The relative standard deviations (RSD) for the mean Z_{mem} in case of α-thrombin titration in presence of 500 μM HSA background is provided in Table 1. This parameter is a measure of reproducibility of the sensor and it is seen that the RSD lies in the range of 9–13%. One possible cause of the RSD could be the error associated with the Ag/AgCl reference electrodes which leech and turn blackish after repeated use of more than 2–3 times. Hence it is advisable to use fresh electrodes and other reference electrode materials may be explored.

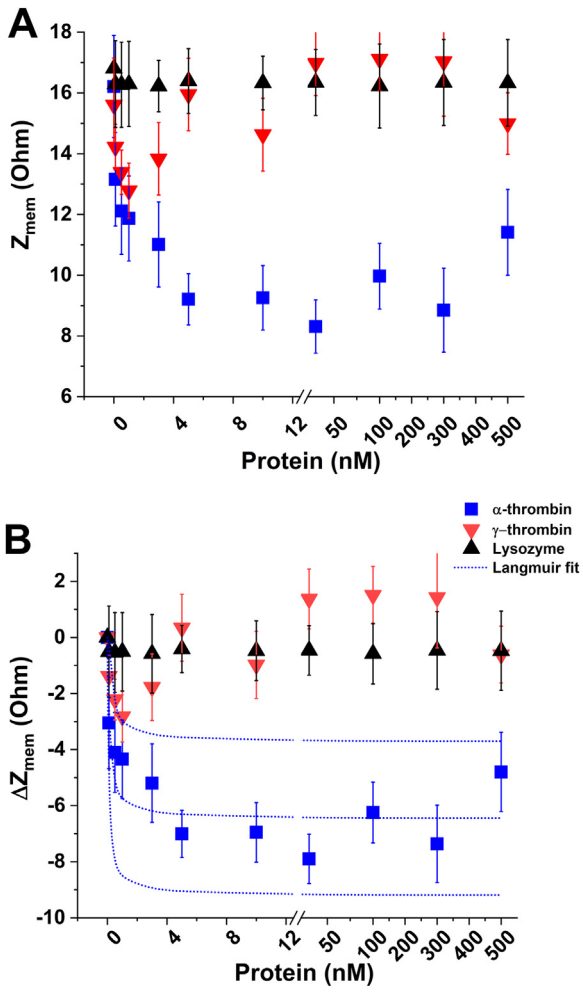

Fig. 3. (A) Z_{mem} and (B) ΔZ_{mem} are plotted for the protein titration in presence of 500 μM HSA as a background in the electrolyte. Impedance is calculated at $f = 100$ Hz. ΔZ_{mem} for the α-thrombin titration is fitted to a Langmuir isotherm to calculate dissociation constant K_D. Each titration experiment was repeated at least 3 times. The error bars correspond to standard deviation of the mean.

Table 1
Standard deviation (SD) and relative standard deviation (RSD) for the mean Z_{mem} for α-thrombin titration in a background of 500 μM HSA.

α-thrombin (nM)	Mean Z_{mem} (Ω)	SD (Ω)	RSD
0	16.21	1.64	0.10
0.01	14.43	1.54	0.11
0.05	13.41	1.21	0.09
0.1	13.16	1.63	0.12
0.5	12.11	1.43	0.12
1	11.87	1.4	0.12
3	11.01	1.4	0.13
5	9.21	0.84	0.09
10	9.26	1.06	0.11
30	8.31	0.88	0.11
100	9.97	1.08	0.11
300	8.85	1.38	0.16
500	11.41	1.41	0.12

3.3. Sensor parameters

The response of the sensor ΔZ_{mem} is proportional to the number of

aptamer-protein complexes formed at each concentration of α-thrombin. The response or calibration curve for α-thrombin in Fig. 3 is fitted to the following 1:1 Langmuir isotherm equation:

$$\Delta Z \quad \propto \quad \Theta = \frac{[\alpha - thrombin]}{[\alpha - thrombin] + K_D} \tag{1}$$

where, Θ = fraction of bound TBA and K_D = dissociation constant for the aptamer-protein complex. The K_D for the TBA/α-thrombin complex in the presence of 500 μM HSA was calculated as 0.18 nM by the Langmuir isotherm fit according to Eq. (1) (shown in Fig. 3B along with confidence interval of 95%). The reported solution K_D for this complex is ~ 3 nM (Daniel et al., 2013). The calculated K_D in the present study is probably lower due to molecular crowding (Nakano et al., 2014) of the aptamer immobilized on the membrane surface. For characterization of the sensor, we denote the absolute value of ΔZ_{mem} as the signal *S*, whereas the response due to blank injections (devoid of any protein) is considered as noise *N*. The signal to noise ratio is thus defined as $S/N = S_{mean}/\sigma_{noise}$, where, S_{mean} is the mean signal and σ_{noise} is the standard deviation of the noise *N*, following the discussions established in previous reports (Morgan and Weber, 1984; Voigtman, 1997; Currie, 1999). The values of S/N obtained for some of the relevant cases are presented in Table 2.

According to Currie (1999) and other reports (Morgan and Weber, 1984; Voigtman, 1997) on electrochemical sensors, an appreciable S/N ratio is 3, which was satisfied by the α-thrombin titration but not satisfied by the γ-thrombin titration, both in the presence of 500 μM HSA. These results are consistent with the selectivity of the sensor towards α-thrombin over other proteins. Also, the S/N ratios for 0.1 nM and 500 nM α-thrombin were higher in the presence of 500 μM HSA compared 0 and 5 μM HSA. It may be noted that the concentration of α-thrombin in a sample could be determined by comparing the sensor response from different dilutions of an α-thrombin solution of unknown concentration against a calibration curve such the Langmuir fit of Fig. 3B.

Table 3 shows how the proposed sensor compares with some other reported approaches/designs. It may be observed that NAAO membrane based impedimetric aptasensors are particularly sensitive to low concentrations of target analyte. The results reported in this study also demonstrate that our approach can be a viable alternative for label-free portable biosensors with minimum requirement of reagents. An aptamer-modified NAAO membrane can also be reused for a second titration of α-thrombin as shown in Supplementary information Fig. S4.

3.4. Discussion of membrane impedance change

Fig. 4A shows the comparison for Z_{mem} during α-thrombin titrations for varying concentrations of HSA (0, 5, and 500 μM) in the electrolyte. It is observed that, in the presence of 0 and 5 μM HSA, the impedance value reached a minimum as the α-thrombin concentration increased

Table 2
Sensor parameters for different test cases.

HSA background	Test protein	Concentration (nM)	S_{mean} (Ohm)	σ_{noise} (Ohm)	S/N
500 μM	α-thrombin	0.1	3.05	0.98	3.12
		30	7.89		7.85
		500	5.08		5.11
500 μM	γ-thrombin	0.1	1.38	0.98	1.41
		30	1.37		1.41
		500	0.98		1.00
5 μM	α-thrombin	0.1	0.4	1.003	0.41
		30	7.8		7.76
		500	1.01		3.98
0 μM	α-thrombin	0.1	0.56	0.37	1.51
		30	3.46		9.24
		500	1.01		2.67

Table 3
Comparison between different sensors for detection of human thrombin.

Sl. No.	Reference	Method	Platform	Detection limit
1	Allsop et al. (2017)	Optical / Surface Plasmon	Aptamer modified metal/semiconductor optic fiber; label free	100 pM in 4.5% w/v Bovine Serum Albumin
2	Lin et al. (2017)	Electrochemical (impedance) / 3-electrode	Aptamer-functionalized MoS2 nanosheet	53 pM in 1% human serum
3	Zhao et al. (2017)	Electrochemical (impedance) / 2-electrode / NAAO membrane	Aminated aptamers grafted on inner wall; label free	1 pM in PBS
3	Goda et al. (2015)	Electrochemical (potentiometry) / 3-electrode / gold microelectrode array	Bivalent aptamer system; label free	5.5 nM in 10 mM MES buffer, pH 6.0
4	Jiang et al. (2014)	Optical / UV–Vis	Aptamer -antibody sandwich; ELISA type sensor	80 pM in PBS
5	de la Escosura-Muñiz et al. (2013)	Electrochemical (voltammetry) / 3-electrode / NAAO membrane	Aptamer-antibody sandwich assay with AuNP tags + silver	5 pM in whole blood (membrane rinsed with PBS after incubation with blood)
6	Xiao et al. (2005)	Electrochemical / 3-electrode / gold disk electrode	Aptamer based using methylene-blue label	64 nM in diluted 50% calf serum
7	This work	Electrochemical (impedance) / 4-electrode / NAAO membrane	Thiolated aptamers; gold coated NAAO; label free	10 pM in presence of 500 μM HSA in PBS

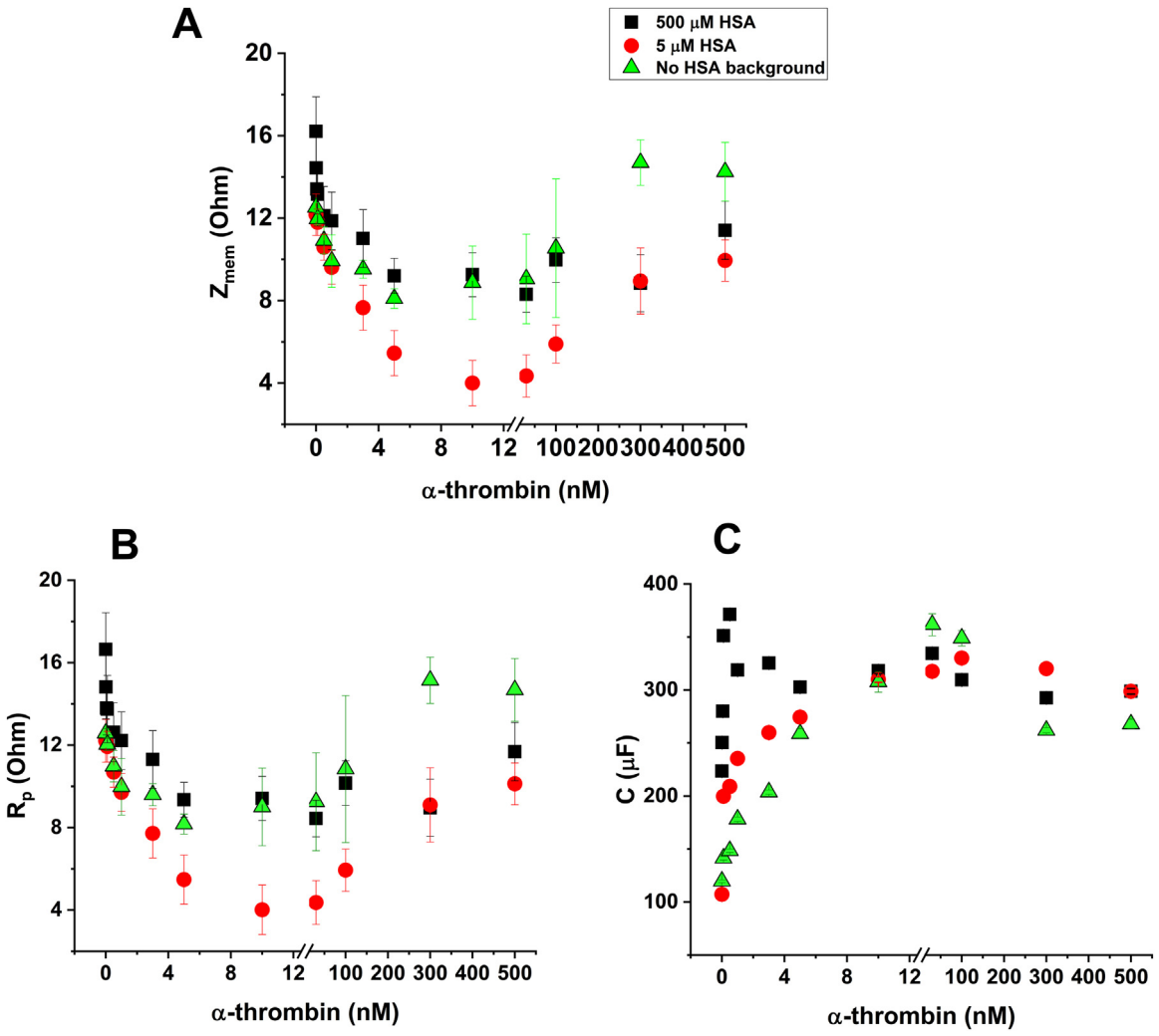

Fig. 4. (A) The membrane impedance Z is plotted for an α-thrombin titration in the presence of 0, 5, and 500 μM HSA. The mean value for each case of background is shown. Impedance is calculated at $f = 100$ Hz. (C) The resistance R_p and (D) capacitance C_{mem} for different backgrounds are shown. Each titration experiment was repeated at least 3 times. The error bars correspond to standard deviation of the mean.

and then increased as the concentration was raised beyond 10 nM. This response of the system resulted in the loss of sensing performance. Particularly, at 0 μM HSA, for very high α-thrombin concentration (e.g. 300 and 500 nM), the impedance is equal/greater than that at the start of the titration. This is because C_{mem} decreased (as it scales inversely with double layer thickness) and R_p increased compared to the value at zero concentration (Figs. 4B and 4C). However, this problem was mostly mitigated with a high concentration (500 μM) of HSA present in the system from the start of titration. The baseline, corresponding to the zero-concentration of titrated α-thrombin, was shifted to a higher value in the presence of 500 μM HSA (Fig. 4A). The average baseline impedances at the start of the experiments were ~16 Ω for 500 μM HSA and ~12–11 Ω for 0 and 5 μM HSA. It is hypothesized that, in the presence of high HSA (500 μM), non-specific adsorption is maximized at the start of the experiment, which increases the baseline. Hence, the sensor can achieve a greater dynamic range and resolution in the presence of high HSA.

NAAO membrane impedance depends on several factors including surface charge density due to the nucleic acids and attached or adsorbed proteins, which is influenced by electrostatic and non-electrostatic interactions (Tagliazucchi et al., 2011; Stein et al., 2004; Wang and Smirnov, 2009). At low bulk salt concentrations, C_{bulk}, compared to the surface charge concentration ΔC on inner nanopore walls and/or on outer surface (Tagliazucchi et al., 2011; Wang and Smirnov, 2009), pore conductance is enhanced (which reduces the impedance) due to a local increase in the counterion concentration required to balance the charges on the grafted biomolecules. The membrane impedance Z_{mem} for pore radius a, porosity α, ion diffusion coefficient D, membrane channel length L, and cross-sectional area A can be expressed by the following expression (Wang and Smirnov, 2009; Vlassiouk et al., 2008).

$$Z_{mem} = \frac{k_B T}{e^2 \alpha D \sqrt{\Delta C^2 + 4C_{bulk}^2}} \frac{L}{A}$$

where e = electron charge, k_B = Boltzmann constant, T = system temperature. For this study, $\Delta C = \frac{N_S}{a} \sim 10^4 \text{M} \gg C_{bulk} = 0.1\text{M}$ where N_s = the surface grafting density of nucleic acids (Ma et al., 2017; Stachowiak et al., 2006), ($\sim 10^{12}$ cm^{-2}), a = membrane pore radius ($\sim 10^{-9}$ m), each of the 50 bases of the TBA has 1 e$^-$ negative charge, and we hypothesize that ΔC increases to a greater extent in response to α-thrombin due to its high affinity for TBA in comparison to the low affinity non-specific interactions with other proteins that bind to a lesser degree. Thus, the pore impedance decreases much more with increasing α-thrombin concentrations compared with proteins with low or no affinity for the aptamer.

In a previous study, Rotem et al. (2012) observed an increase in current through a TBA-modified single nanopore on binding with α-thrombin, suggesting a concomitant decrease in the pore impedance, which supports our observation. They argued that ion flow through the

nanopores could be affected due to the biomolecular surface charge as well as by the configurational change of aptamer at the pore entrance due to binding with α-thrombin. However, with increasing numbers of α-thrombin-TBA complexes, giving rise to greater steric hindrance to ion flow across the nanochannels of the membrane, the mechanism of "volume exclusion" (Vlassiouk et al., 2005) will dominate over the "surface-charge" mechanism (Wang and Smirnov, 2009). The result will be a decrease in conductance and thus an increase in membrane impedance. In the event of membrane impedance being dictated by volume exclusion the pore resistance R_p increases and can be expressed as below (Kant et al., 2014b; Siwy and Fuliński, 2004),

$$R_p = \frac{L}{\pi \Lambda a^2}$$

where Λ is the specific conductivity of the electrolyte in the nanochannel. If we consider that Λ is unchanged, then the abundance of protein-aptamer complexes can reduce the effective pore radius and thus increase R_p. This could explain the increase in R_p, which in turn increases Z_{mem}, at very high concentrations of α-thrombin. We observed more of this effect (Figs. 4B and 4C) in the presence of 0 and 5 μM HSA at 300 and 500 nM α-thrombin. Karnik et al. (2005, 2007) also showed that, with increasing complex formation, the conductance decreases after a certain point and impedance starts increasing due to larger steric effects.

The previous discussion considers surface charge effects on nanochannels but in the real scenario the nucleic acid-protein complex is, in effect, a polyelectrolyte layer and thus the sizes and shapes of the biomolecules must be considered to provide a thorough explanation for the conductance change. Tagliazucchi et al. (2013) reported that polyelectrolytes on the outer surface of the nanopores, compared to those on inner walls, can lead to equal or better rectification of ionic current, depending on biomolecules charge and ionic concentration. The NAAO membrane used in this study were sputter coated with a ~60 nm thick film of gold. Due to the physical deposition process most of the gold was accumulated on the mouth of the nanopores, with much less penetration into the nanochannels. Thus, the thiolated aptamers were likely aggregated around and closer to the mouth of the pore.

Interestingly, Zhao et al. (2017) immobilized aptamers throughout the inner surface of the nanopores and demonstrated an increase in impedance with formation of α-thrombin-aptamer complexes inside the NAAO membrane, for their scheme of sensor arrangement. However, they did not report the detection of the analyte/target in presence of high concentrations of other proteins of low affinity for the aptamer such as HSA, which we have demonstrated in the present study. The nature of the impedance change described in the present study is opposite of that discussed in the work by Zhao et al. (2017) Though previous literature (Vlassiouk et al., 2008; Rotem et al., 2012; Siwy and Fuliński, 2004; Karnik et al., 2005, 2007; Tagliazucchi et al., 2013), as described above, support our observations, it is to be noted that these authors only considered the instance of receptor-target interaction. Thus, it is still not clear how the presence of high concentrations of HSA improves the sensitivity in our study. This effect of HSA demands greater inspection of the interaction of proteins with aptamers grafted to nanoporous membranes and to other exposed portions of the membranes, such as the hexanol-modified gold surface. Computational modeling considering buffer composition, biomolecule configurations and charge might reveal the exact physics of the system.

4. Conclusion

In this study we have established a sensitive and selective aptamer-functionalized NAAO membrane sensor for α-thrombin detection. We have shown that it is possible to detect α-thrombin in presence of high concentration HSA by using aptamers functionalized on gold coated NAAO membranes and the four-electrode impedance spectroscopy. We also found that increasing the HSA background in the electrolyte increased the baseline impedance, possibly through the saturation of the available sites for non-specific adsorption, which in turn improved the S/N ratio and enabled low concentration analyte detection. It may be seen from the results that even though the sensor has a detection limit of 10 pM (based on S/N ratio > 3), the error bars due to the negative control γ-thrombin overlap with the confidence interval for α-thrombin, below 2 nM titrations, and the RSD for α-thrombin varies between 9% and 13%. This scheme of detection may be extended to other protein-ligand systems to further establish its efficacy with tests carried out in serum samples. The sensor could also be utilized in point-of-care diagnostics development due to the advantages offered by portable impedance analyzers.

Acknowledgement

The work was supported by the Grant no. 2R44DK098031 to Aptalogic Inc. from the National Institutes of Health. Helpful discussions regarding the execution of the experiments and aptamer biochemistry with Dr. Muslum Ilgu, Dr. Soma Banerjee-Singh and Dr. Shambhavi Shubham are gratefully acknowledged.

Competing financial interests

M.N.H owns Aptalogic Inc.

Author contributions

A.G. conducted the literature review and designed the experiments. A.G and B.Y. conducted the experiments and analyzed the data. All authors wrote, reviewed and edited the manuscript extensively.

Appendix A. Supporting information

Supplementary data associated with this article can be found in the online version at doi:10.1016/j.bios.2018.10.010.

References

Allsop, T., Mou, C., Neal, R., Mariani, S., Nagel, D., Tombelli, S., Poole, A., Kalli, K., Hine, A., Webb, D.J., Culverhouse, P., Mascini, M., Minunni, M., Bennion, I., 2017. Real-time kinetic binding studies at attomolar concentrations in solution phase using a single-stage opto-biosensing platform based upon infrared surface plasmons. Opt. Express 25 (1), 39–58.

Aronson, D.L., Stevan, L., Ball, A.P., Franza, B.R., Finlayson, J.S., 1977. Generation of the combined prothrombin activation peptide (F1-2) during the clotting of blood and plasma. J. Clin. Investig. 60 (6), 1410–1418.

Bock, C.L., Griffin, C.L., Latham, A.J., Vermass, H.E., Toole, J.J., 1992. Selection of single stranded DNA molecules that bind and inhibit human thrombin. Nature 355.

Chaturvedi, P., Rodriguez, S.D., Vlassiouk, I., Hansen, I.A., Smirnov, S.N., 2016. Simple and versatile detection of viruses using anodized alumina membranes. ACS Sens. 1 (5), 488–492.

Currie, L.A., 1999. Detection and quantification limits: origins and historical overview1 adapted from the proceedings of the 1996 joint statistical meetings (American statistical Association, 1997). Original title: "foundations and future of detection and quantification limits". contribution of the National Institute of Standards and technology; not subject to copyright.1. Anal. Chim. Acta 391 (2), 127–134.

Daniel, C., Roupioz, Y., Gasparutto, D., Livache, T., Buhot, A., 2013. Solution-phase vs Surface-phase aptamer-protein affinity from a label-free kinetic biosensor. PLoS One 8 (9), e75419.

Daniels, J.S., Pourmand, N., 2007. Label-free impedance biosensors: opportunities and challenges. Electroanalysis 19 (12), 1239–1257.

Deng, B., Lin, Y., Wang, C., Li, F., Wang, Z., Zhang, H., Li, X.-F., Le, X.C., 2014. Aptamer binding assays for proteins: the thrombin example—a review. Anal. Chim. Acta 837 (Supplement C), 1–15.

Du, Y., Dong, S., 2017. Nucleic acid biosensors: recent advances and perspectives. Anal. Chem. 89 (1), 189–215.

de la Escosura-Muñiz, A., Merkoçi, A., 2010. Label-free voltammetric immunosensor using a nanoporous membrane based platform. Electrochem. Commun. 12 (6), 859–863.

de la Escosura-Muñiz, A., Chunglok, W., Surareungchai, W., Merkoçi, A., 2013. Nanochannels for diagnostic of thrombin-related diseases in human blood. Biosens. Bioelectron. 40 (1), 24–31.

Goda, T., Higashi, D., Matsumoto, A., Hoshi, T., Sawaguchi, T., Miyahara, Y., 2015. Dual aptamer-immobilized surfaces for improved affinity through multiple target binding

in potentiometric thrombin biosensing. Biosens. Bioelectron. 73, 174–180.
Ilgu, M., Nilsen-Hamilton, M., 2016. Aptamers in analytics. Analyst 141 (5), 1551–1568.
Jiang, Z., Yang, T., Liu, M., Hu, Y., Wang, J., 2014. An aptamer-based biosensor for sensitive thrombin detection with phthalocyanine@SiO2 mesoporous nanoparticles. Biosens. Bioelectron. 53, 340–345.
Kant, K., Priest, C., Shapter, J.G., Losic, D., 2014a. The influence of nanopore dimensions on the electrochemical properties of nanopore arrays studied by impedance spectroscopy. Sens. 14 (11), 21316–21328.
Kant, K., Yu, J., Priest, C., Shapter, J.G., Losic, D., 2014b. Impedance nanopore biosensor: influence of pore dimensions on biosensing performance. Analyst 139 (5), 1134–1140.
Karnik, R., Castelino, K., Fan, R., Yang, P., Majumdar, A., 2005. Effects of biological reactions and modifications on conductance of nanofluidic channels. Nano Lett. 5 (9), 1638–1642.
Karnik, R., Duan, C., Castelino, K., Daiguji, H., Majumdar, A., 2007. Rectification of ionic current in a nanofluidic diode. Nano Lett. 7 (3), 547–551.
Kumeria, T., Santos, A., Losic, D., 2014. Nanoporous anodic alumina platforms: engineered surface chemistry and structure for optical sensing applications. Sensors 14 (7).
Li, X., Shen, L., Zhang, D., Qi, H., Gao, Q., Ma, F., Zhang, C., 2008. Electrochemical impedance spectroscopy for study of aptamer–thrombin interfacial interactions. Biosens. Bioelectron. 23 (11), 1624–1630.
Li, X., Zhai, T., Gao, P., Cheng, H., Hou, R., Lou, X., Xia, F., 2018a. Role of outer surface probes for regulating ion gating of nanochannels. Nat. Commun. 9 (1), 40.
Li, X., Zhang, T., Gao, P., Wei, B., Jia, Y., Cheng, Y., Lou, X., Xia, F., 2018b. Integrated solid-state nanopore electrochemistry array for sensitive, specific, and label-free biodetection. Langmuir.
Lin, K.-C., Jagannath, B., Muthukumar, S., Prasad, S., 2017. Sub-picomolar label-free detection of thrombin using electrochemical impedance spectroscopy of aptamer-functionalized MoS2. Analyst 142 (15), 2770–2780.
Ma, X., Gosai, A., Balasubramanian, G., Shrotriya, P., 2017. Aptamer based electrostatic-stimuli responsive surfaces for on-demand binding/unbinding of a specific ligand. J. Mater. Chem. B 5 (20), 3675–3685.
Macias, G., Hernández-Eguía, L.P., Ferré-Borrull, J., Pallares, J., Marsal, L.F., 2013. Gold-coated ordered nanoporous anodic alumina bilayers for future label-free Interferometric biosensors. ACS Appl. Mater. Interfaces 5 (16), 8093–8098.
Morgan, D.M., Weber, S.G., 1984. Noise and signal-to-noise ratio in electrochemical detectors. Anal. Chem. 56 (13), 2560–2567.
Nakano, S.-i., Miyoshi, D., Sugimoto, N., 2014. Effects of molecular crowding on the structures, interactions, and functions of nucleic acids. Chem. Rev. 114 (5), 2733–2758.
Rai, V., Deng, J., Toh, C.-S., 2012. Electrochemical nanoporous alumina membrane-based label-free DNA biosensor for the detection of Legionella sp. Talanta 98, 112–117.
Rotem, D., Jayasinghe, L., Salichou, M., Bayley, H., 2012. Protein detection by nanopores equipped with aptamers. J. Am. Chem. Soc. 134 (5), 2781–2787.
Santos, A., Kumeria, T., Losic, D., 2013. Nanoporous anodic aluminum oxide for chemical sensing and biosensors. TrAC Trends Anal. Chem. 44 (Supplement C), 25–38.
Schultze, P., Macaya, R.F., Feigon, J., 1994. Three-dimensional solution structure of the thrombin-binding DNA Aptamer d(GGTTGGTGTGGTTGG). J. Mol. Biol. 235 (5), 1532–1547.
Siwy, Z., Fuliński, A., 2004. A nanodevice for rectification and pumping ions. Am. J. Phys. 72 (5), 567–574.
Stachowiak, J.C., Yue, M., Castelino, K., Chakraborty, A., Majumdar, A., 2006. Chemomechanics of surface stresses induced by DNA hybridization. Langmuir 22 (1), 263–268.
Stein, D., Kruithof, M., Dekker, C., 2004. Surface-charge-governed ion transport in nanofluidic channels. Phys. Rev. Lett. 93 (3), 035901.
Tagliazucchi, M., Rabin, Y., Szleifer, I., 2011. Ion transport and molecular organization are coupled in polyelectrolyte-modified nanopores. J. Am. Chem. Soc. 133 (44), 17753–17763.
Tagliazucchi, M., Rabin, Y., Szleifer, I., 2013. Transport rectification in nanopores with outer membranes modified with surface charges and polyelectrolytes. ACS Nano 7 (10), 9085–9097.
Tan, F., Leung, P.H.M., Liu, Z.-b., Zhang, Y., Xiao, L., Ye, W., Zhang, X., Yi, L., Yang, M., 2011. A PDMS microfluidic impedance immunosensor for E. coli O157:H7 and Staphylococcus aureus detection via antibody-immobilized nanoporous membrane. Sens. Actuators B Chem. 159 (1), 328–335.
Toccafondi, C., Proietti Zaccaria, R., Dante, S., Salerno, M., 2016. Fabrication of gold-coated ultra-thin anodic porous alumina substrates for augmented SERS. Materials 9 (6).
Vlassiouk, I., Takmakov, P., Smirnov, S., 2005. Sensing DNA hybridization vIa ionic conductance through a nanoporous electrode. Langmuir 21 (11), 4776–4778.
Vlassiouk, I., Smirnov, S., Siwy, Z., 2008. Ionic selectivity of single nanochannels. Nano Lett. 8 (7), 1978–1985.
Voigtman, E., 1997. Comparison of signal-to-noise ratios. Anal. Chem. 69 (2), 226–234.
Wang, L., Liu, Q., Hu, Z., Zhang, Y., Wu, C., Yang, M., Wang, P., 2009. A novel electrochemical biosensor based on dynamic polymerase-extending hybridization for E. coli O157:H7 DNA detection. Talanta 78 (3), 647–652.
Wang, R.E., Tian, L., Chang, Y.-H., Homogeneous Fluorescent, A., 2012. Sensor for human serum albumin. J. Pharm. Biomed. Anal. 63, 165–169.
Wang, X., Smirnov, S., 2009. Label-free DNA sensor based on surface charge modulated ionic conductance. ACS Nano 3 (4), 1004–1010.
Xiao, Y., Lubin Arica, A., Heeger Alan, J., Plaxco Kevin, W., 2005. Label-free electronic detection of thrombin in blood serum by using an aptamer-based sensor. Angew. Chem. Int. Ed. 44 (34), 5456–5459.
Ye, W.W., Shi, J.Y., Chan, C.Y., Zhang, Y., Yang, M., 2014. A nanoporous membrane based impedance sensing platform for DNA sensing with gold nanoparticle amplification. Sens. Actuators B Chem. 193, 877–882.
Zhao, X.-P., Cao, J., Nie, X.-G., Wang, S.-S., Wang, C., Xia, X.-H., 2017. Label-free monitoring of the thrombin–aptamer recognition reaction using an array of nanochannels coupled with electrochemical detection. Electrochem. Commun. 81 (Supplement C), 5–9.